The Journal of Chemical Physics ARTICLE scitation.org/journal/jcp

Proton-transfer spectroscopy beyond the normal-mode scenario

Cite as: J. Chem. Phys. 157, 174116 (2022); doi: 10.1063/5.0116686
Submitted: 29 July 2022 • Accepted: 26 September 2022 •
Published Online: 7 November 2022

Florian N. Brünig,[1] Paul Hillmann,[1] Won Kyu Kim,[2] Jan O. Daldrop,[1] and Roland R. Netz[1,a)]

AFFILIATIONS

[1] Department of Physics, Freie Universität Berlin, 14195 Berlin, Germany
[2] School of Computational Sciences, Korea Institute for Advanced Study, Seoul 02455, Republic of Korea

[a)] Author to whom correspondence should be addressed: rnetz@physik.fu-berlin.de

ABSTRACT

A stochastic theory is developed to predict the spectral signature of proton-transfer processes and is applied to infrared spectra computed from *ab initio* molecular-dynamics simulations of a single $H_5O_2^+$ cation. By constraining the oxygen atoms to a fixed distance, this system serves as a tunable model for general proton-transfer processes with variable barrier height. Three spectral contributions at distinct frequencies are identified and analytically predicted: the quasi-harmonic motion around the most probable configuration, amenable to normal-mode analysis, the contribution due to transfer paths when the proton moves over the barrier, and a shoulder for low frequencies stemming from the stochastic transfer-waiting-time distribution; the latter two contributions are not captured by normal-mode analysis but exclusively reported on the proton-transfer kinetics. In accordance with reaction rate theory, the transfer-waiting-contribution frequency depends inversely exponentially on the barrier height, whereas the transfer-path-contribution frequency is rather insensitive to the barrier height.

I. INTRODUCTION

The transfer dynamics of excess protons in the aqueous environment is central to many biochemical processes,[1] but despite substantial work, even for acidic water, a complete kinetic model that would describe all spectral features encompassing the low THz and infrared (IR) regimes remains elusive. Typically, the discussion is based on two idealized proton-transfer intermediates, namely the $H_5O_2^+$ Zundel cation, where two water molecules symmetrically point their oxygens to the excess proton,[2] and the Eigen cation, where hydronium H_3O^+ is formed and solvated by three water molecules.[3] Accordingly, proton diffusion in water is portrayed as a stochastic succession of these two states, where the excess proton switches during diffusion: It is a defect that diffuses rather than a specific proton, which explains the high proton mobility in water.[4,5]

An intensely debated question concerns the relative stability and abundance of the Eigen and Zundel forms in acidic water.[6–10] Several experimental 2D IR studies suggest the Zundel form dominates the proton-transfer spectroscopic signature in bulk water.[8,9,11–14] From *ab initio* molecular-dynamics (AIMD) work, it was concluded that an excess proton in bulk liquid water is predominantly present in the Eigen state and that the Zundel form plays the role of a relatively short-lived transfer or barrier state.[15–17] As the separation between the two water oxygen atoms that flank the excess proton decreases, the relative stability changes and eventually the Zundel form becomes preferred over the Eigen form,[18] it transpires that excess proton and water motion are dynamically coupled. As a consequence, proton transfer from one water molecule to a neighboring one not only involves motion of the proton but also of the flanking water molecules and even further water neighbors, making the kinetics highly collective.[7,10,13,14,16,19–23]

In isolated $H_5O_2^+$ clusters, the subject of this paper, and protonated water wires the situation is different from bulk: Experimental[8,24–27] and theoretical[19,20,28–33] work demonstrated that the oxygen–oxygen distance is decreased and the Zundel form is more stable than the hydronium form. By chemical modifications of two proton acceptors in gas-phase clusters, proton-transfer energy barriers of variable heights could be demonstrated.[34] Proton-transfer barriers also exist inside proteins, where amino-acid

side chains that act as proton donors can be located at variable separations.[35–38] Thus, energetic barriers for proton transfer exist in a variety of systems and produce characteristic spectroscopic signatures that fundamentally go beyond the established normal-mode picture, as we show in this paper.

The excess proton has a high net charge and during a transfer event covers significant distances over short times; consequently, IR linear and nonlinear spectroscopy are very suitable methods to detect proton-transfer events and have been applied to bulk acidic solutions,[2] acidic water clusters,[34] gas-phase ions,[39] and proteins.[40] While spectra computed from dynamical simulations encompass nonlinear dynamics and do not employ a normal-mode approximation, the interpretation of simulated spectra is typically based on normal modes, with notable extensions to include anharmonic and frequency-dependent friction effects.[41–43] Also the interpretation of experimental spectra is traditionally based on normal-mode analysis around one or multiple local energy minima, where the normal-mode frequency f_{NM} defines a vibrational time scale according to $\tau_{\mathrm{NM}} = 1/f_{\mathrm{NM}}$. However, if a barrier exists, two additional time scales emerge, the transfer-waiting time τ_{TW}, which is the time the proton waits in one minimum before it transfers,[44–46] and the transfer-path (TP) time τ_{TP}, which is the time the actual transfer over the barrier takes.[47–51]

In this paper, we show by a combination of stochastic theory and *ab initio* molecular-dynamics (AIMD) simulations that the normal-mode, the transfer-waiting, and the TP time scales, which together characterize the transfer-waiting kinetics, leave distinct and characteristic spectroscopic traces. As a specific example, we consider a $H_5O_2^+$ cation in gas phase. In order to probe different proton-transfer barrier heights, we constrain the separation between the two water oxygen atoms at variable fixed distances, which is applicable to proteins and other systems where proton-accepting residues are positioned at well-defined distances.[35–37] While the transfer-waiting time depends exponentially on the barrier height U_0 as $\tau_{\mathrm{TW}} \sim e^{U_0/k_BT}$,[44,46] the normal-mode time scale τ_{NM} is determined by the stiffness of the effective harmonic potential k and the effective mass m according to $\tau_{\mathrm{NM}} = 2\pi\sqrt{m/k} \sim 1/\sqrt{U_0}$, and the TP time depends logarithmically on U_0 as $\tau_{\mathrm{TP}} \sim \ln(U_0/k_BT)/U_0$.[49–51] From the different functional dependencies on U_0, one expects a not too low barrier heights $\tau_{\mathrm{NM}} \sim \tau_{\mathrm{TP}} < \tau_{\mathrm{TW}}$. Indeed, for an oxygen–oxygen distance of $R_{\mathrm{OO}} = 2.64$ Å, which in our AIMD simulations of the $H_5O_2^+$ cation leads to a moderate effective barrier height of $U_0 = 2.0\ k_BT$, the normal-mode spectroscopic contributions lie between 1000 and 2000 cm^{-1}, the TP contribution turns out to be a rather well-defined band centered around 800 cm^{-1}, and since the waiting-time distribution is rather broad, the transfer-waiting contribution forms a continuum band below 500 cm^{-1} that reaches deep into the GHz range, in agreement with experimental THz absorption measurements.[52,53]

Our AIMD results show that the broad low-frequency transfer-waiting spectral contribution crucially depends on the barrier height, controlled by the relative distance of the water molecules sharing the excess proton. In contrast, the TP spectral contribution shifts only slightly with barrier height, in agreement with recent theoretical and experimental findings.[49–51] Isotope exchange of the excess proton, on the other hand, affects the TP contribution but not the waiting-time contribution, as we predict by stochastic theory. In summary, we show that the spectroscopic signature of proton barrier crossing reflects transfer-waiting statistics as well as TP kinetics and, in particular, cannot be modeled by a succession of normal modes located across the barrier. Our results also apply to experimental systems with fluctuating barrier heights, such as acidic water, as recently considered by a combined theoretical/experimental study:[53] We show that the spectrum of unconstrained $H_5O_2^+$ can be quite accurately reproduced by Boltzmann averaging of spectra of constrained systems; thus, all of the features we see in our constrained simulations are also expected in experimental systems where the proton acceptor separation can fluctuate.

Our simulations are performed at the Born–Oppenheimer level with classically treated nuclei. Nuclear-quantum zero-point motion has been shown to lead to an increased proton density at the barrier, which is typically interpreted as a signature of a decreased barrier height,[10,15,16,28,54] but for large enough barriers, such nuclear-quantum effects are not expected to eliminate the spectroscopic features we predict, as discussed in the supplementary material, Sec. I. Furthermore, electron-nuclear quantum-mechanical coupling has been shown to be relevant for protonated systems[30] but is challenging to include within the framework of our stochastic theory and therefore, left for future work.

II. RESULTS AND DISCUSSION

We perform AIMD simulations of a single $H_5O_2^+$ cation with a total trajectory length of 5 ns for several constrained oxygen separations as well as for unconstrained oxygens (see Sec. III A for details). Suitable reaction coordinates are the oxygen–oxygen distance R_{OO} and the excess-proton distance from the oxygen midpoint position, $d = \frac{1}{2}(R_{\mathrm{O_1H}} - R_{\mathrm{O_2H}})_x$, projected onto the x-axis that connects the two oxygens, as illustrated in Fig. 1(a). The two-dimensional free energy in Fig. 1(d), calculated from the probability distribution of unconstrained simulations according to $U(R_{\mathrm{OO}}, d) = -k_BT \ln p(R_{\mathrm{OO}}, d)$, demonstrates that the global minimum of the free energy is located around $R_{\mathrm{OO}} = 2.40$ Å, and $d = 0$. This is the symmetric Zundel state, where the excess proton is symmetrically shared by the oxygens.[2] For $R_{\mathrm{OO}} > 2.55$ Å, a double-well free-energy landscape along d appears, which indicates a preferred localization of the excess proton near one water molecule, analogous to the Eigen state in bulk water.[3] The excess proton trajectory for constrained $R_{\mathrm{OO}} = 2.64$ Å in Fig. 1(b) is typical for the thermally activated barrier crossing of a weakly damped massive particle[46] and involves a moderate barrier height of $U_0 = 2.0\,k_BT$, as seen in the corresponding free-energy profile in Fig. 1(c). Most of the time, the excess proton is part of a H_3O^+ molecule and vibrates in one of the two free-energy minima with an oscillation time described by the normal-mode time $\tau_{\mathrm{NM}} = 17$ fs [inset Fig. 1(b)], while from time to time the proton suddenly crosses the barrier, the mean time of such a TP is $\tau_{\mathrm{TP}} = 25$ fs [inset Fig. 1(b)]. The longest time scale is the transfer-waiting time, which for $R_{\mathrm{OO}} = 2.64$ Å is $\tau_{\mathrm{TW}} = 440$ fs. In Fig. 1(e), we show as a grey solid line the absorption spectrum of the unconstrained $H_5O_2^+$ cation for an electric field along x, the oxygen separation direction, calculated from the entire nuclear and electronic polarizations (see Sec. III A). It shows, in addition to the OH stretch and HOH bend bands at 3400 and 1800 cm^{-1}, respectively, a prominent feature at 1000 cm^{-1}, which is the Zundel normal mode, where the excess proton vibrates in a rather soft potential produced by the two flanking water molecules (see the supplementary material, Secs. II and III, for

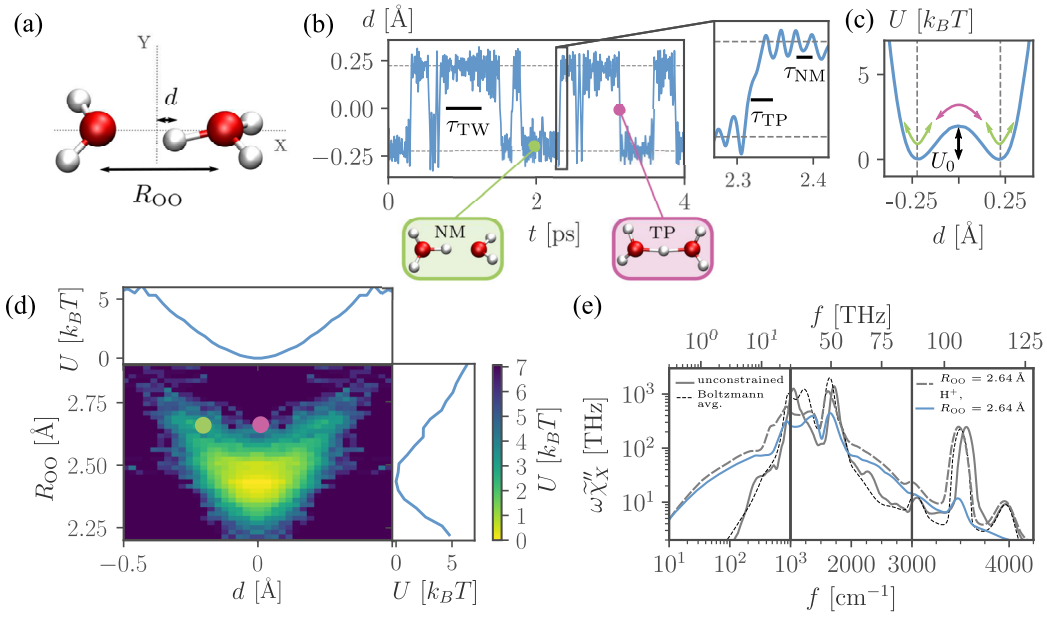

FIG. 1. *Ab initio* molecular-dynamics (AIMD) simulations of the $H_5O_2^+$ cation. (a) The oxygen–oxygen separation R_{OO} and the proton distance from the oxygen midpoint along the *x* axis, named *d*, describe the excess-proton dynamics. (b) The excess proton trajectory for fixed R_{OO} = 2.64 Å visualizes the transfer-waiting time τ_{TW} as well as the normal-mode time τ_{NM} and the transfer-path (TP) time τ_{TP} (see the inset). Selected snapshots show structures at the free-energy minimum and at the barrier top. (c) Free-energy profile for fixed R_{OO} = 2.64 Å, extracted from constrained simulations. (d) 2D free-energy landscape in terms of R_{OO} and *d* from unconstrained simulations. (e) Absorption spectra for an E field along the *x* axis where $\omega = 2\pi f$. The grey solid line shows the total (i.e., nuclear + electronic) spectrum of the unconstrained system, compared with the Boltzmann average of constrained systems (black broken line). The grey broken line shows the total spectrum for constrained R_{OO} = 2.64 Å, compared to the spectrum of only the excess proton (blue line, multiplied by a factor of 2). Note the change of scales at f = 1000 cm^{-1} and f = 3000 cm^{-1}.

a literature overview). The spectrum for the constrained system with R_{OO} = 2.64 Å, grey broken line, displays a band at 800 cm^{-1} and a very broad shoulder that extends down to the lowest frequencies. As we show in this paper, these two spectral features stem from proton TPs and proton transfer-waiting-time stochastics, respectively, and are the only spectroscopic contributions that reflect the actual proton-transfer kinetics. Interestingly, the spectral contribution of only the excess proton for fixed R_{OO} = 2.64 Å (blue solid line, multiplied by a factor of 2) is almost identical to the full spectrum (gray broken line), so we conclude that the IR spectrum is predominantly caused by proton motion and can thus be used to investigate excess-proton dynamics (more details are given in the supplementary material, Sec. IV). In fact, the spectrum of the unconstrained system (gray solid line) agrees well with the free-energy-weighted Boltzmann average over constrained spectra with different R_{OO} values (black broken line, see the supplementary material, Sec. V, for details), indicating that the absorption spectrum can be understood from decoupled proton and oxygen dynamics. Our simulation model with constrained oxygen–oxygen separation is thus also a tool to decompose and, thereby, understand unconstrained system spectra (a finding that is obvious only for static observables[55]).

In order to distinguish transfer-waiting, TP and normal-mode spectral contributions, the proton trajectory $d(t)$ is decomposed according to $d(t) = d_{TW}(t) + d_{TP}(t) + d_{NM}(t)$, as illustrated in Fig. 2(a) for R_{OO} = 2.64 Å. The transfer-waiting part $d_{TW}(t)$ describes two-state kinetics with instantaneous transfers when the trajectory last crosses a free-energy minimum at $d^*_{TW} = \pm 0.22$ Å. The TP contribution $d_{TP}(t)$ consists of transfer trajectories between last and first crossing the free-energy minima, including recrossings where the proton shuttles repeatedly back and forth between the minima. Recrossings are rather frequent for the low friction experienced by the proton[46] (see the supplementary material, Sec. VI), a threefold recrossing event is seen in the proton trajectory in Fig. 2(a) at t = 0.6 ps. Finally, the normal-mode part $d_{NM}(t)$ comprises the trajectory remainder.

Figure 2(b) shows in blue the simulated excess-proton spectrum decomposed into its three components according to $\tilde{\chi}'' = \tilde{\chi}''_B + \tilde{\chi}''_{TP} + \tilde{\chi}''_{NM}$, the red broken lines show theoretical predictions (which will be explained further below). Trajectory decomposition in the time domain creates spectral cross contributions, which are relatively small, as shown in the supplementary material, Secs. VII and VIII, and are added to $\tilde{\chi}''_{NM}$. The transfer-waiting spectrum $\tilde{\chi}''_{TW}$ in Fig. 2(b2) displays a pronounced low-frequency shoulder, which reflects the transfer-waiting-time distribution. The TP spectrum $\tilde{\chi}''_{TP}$ in Fig. 2(b3) is a rather well defined band at 800 cm^{-1}. Even though the time fraction the excess proton spends on TPs is only 16% for R_{OO} = 2.64 Å, the spectral contribution is significant due to the large and quick charge displacement: The proton transfer velocity of roughly $v_{TP} = 2d^*_{TP}/\tau_{TP} = 0.44$ Å/25 fs = 1.8×10^3 m/s is slightly larger than the proton thermal velocity of $v_{th} = \sqrt{k_BT/m_p}$

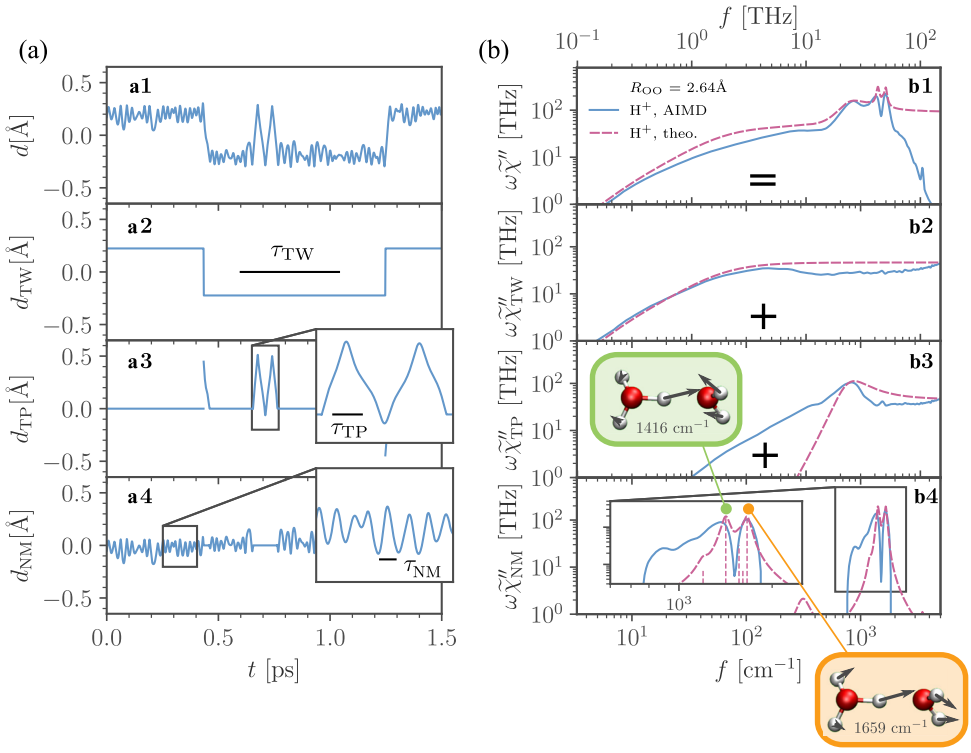

FIG. 2. AIMD simulations of a $H_5O_2^+$ cation with constrained R_{OO} = 2.64 Å. (a) Decomposition of the excess-proton trajectory $d(t)$ into the two-state transfer-waiting contribution $d_{TW}(t)$, the TP contribution $d_{TP}(t)$ and the remaining normal-mode contribution $d_{NM}(t)$. (b) Blue solid lines show the simulated excess-proton spectrum $\omega\tilde{\chi}''$ and its decomposition into the transfer-waiting $\omega\tilde{\chi}''_{TW}$, the TP $\omega\tilde{\chi}''_{TP}$ and the normal-mode contribution $\omega\tilde{\chi}''_{NM}$. The red broken lines in (b2) and (b3) show the corresponding theoretical predictions according to Eqs. (1) and (5). The red broken line in (b4) shows the normal-mode spectrum including friction-induced line broadening. The snapshots illustrate the two dominant normal modes at 1416 and 1659 cm^{-1}.

= 1.5×10^3 m/s, where $m_p = 1.7 \times 10^{-27}$ kg is the proton mass. This confirms previous findings that TPs correspond to the high-energetic part of the Maxwell–Boltzmann ensemble, i.e., the excess proton initiates a TP only when its kinetic energy is significantly above average.[56] The normal-mode spectrum $\tilde{\chi}''_{NM}$ in Fig. 2(b4) consists of two main peaks.

We will now present analytic theories for each simulated spectral contribution shown in Figs. 2(b2)–2(b4). A stochastic two-state process has the spectrum

$$\omega\tilde{\chi}''_{TW}(\omega) = \frac{2q^2 {d^*_{TW}}^2}{V\epsilon_0 k_B T}\ \mathrm{Re}\left(\frac{\omega^2 \tilde{q}_{TW}(\omega)}{1-\tilde{p}_{TW}(\omega)^2}\right) \tag{1}$$

and depends on the Fourier-transformed transfer-waiting-time distribution $\tilde{p}_{TW}(\omega)$ and the survival distribution $\tilde{q}_{TW}(\omega)$, which is defined as $q_{TW}(t) = \int_t^\infty p_{TW}(t')dt'$, the positions of the free-energy minima $\pm d^*_{TW}$, the excess proton charge $q = e$ and the system volume V (see the supplementary material, Sec. IX, for a detailed derivation). Using d^*_{TW} = 0.22 Å and bi-exponential fits for $p_{TW}(t)$ to the simulation data in Fig. 4(c), $\omega\tilde{\chi}''_{TW}(\omega)$ according to Eq. (1) (red broken line) matches the simulation data (blue solid line) in Fig. 2(b2) very well without any fitting parameters. For a single-exponential waiting-time distribution, $p_{TW}(t) = \tau_{TW}^{-1} \exp(-t/\tau_{TW})$, Eq. (1) simplifies to

$$\omega\tilde{\chi}''_{TW}(\omega) = \frac{2q^2 {d^*_{TW}}^2}{V\epsilon_0 k_B T}\frac{\tau_{TW}\omega^2}{(4+\tau_{TW}^2\omega^2)}, \tag{2}$$

which shows that the spectrum is identical to an overdamped harmonic oscillator with a corner frequency $\omega^*_{TW} \sim 1/\tau_{TW}$ (see the supplementary material, Sec. X, for details). For large frequencies, $\omega\tilde{\chi}''_{TW}$ is constant and proportional to the transfer-waiting rate, $\omega\tilde{\chi}''_{TW} \sim 1/\tau_{TW}$, for small frequencies $\omega\tilde{\chi}''_{TW} \sim \tau_{TW}\,\omega^2$.

The TP spectral contribution depends on the TP shape. The ensemble of all 2829 TPs observed in the simulations for R_{OO} = 2.64 Å is shown in Fig. 3(a) (gray lines), together with the mean TP (blue solid line) obtained by position averaging. The path-integral saddle-point prediction for the TP shape over a parabolic barrier,[51]

$$d_{TP}(t) = d^*_{TW}\left[e^{t/\kappa} - e^{-t/\kappa}\right]/\mathcal{N} \tag{3}$$

(red dotted line), matches the simulated mean TP shape very well ($\mathcal{N}$ is a normalization constant). In the supplementary material, Sec. XI, it is shown that Eq. (3) corresponds to the exact mean TP shape in the high-barrier limit.[50] The fitted characteristic time $\kappa = {d^*_{TW}}^2\gamma/(2U_0)$ = 6.5 fs depends on the effective friction coefficient γ acting on the proton as it moves over the barrier. A straight line (black broken line) also describes the simulated mean TP shape quite well. Figure 3(b) shows the TP-time distribution of all TPs (green triangles) together with a decomposition into single (non-recrossing, blue squares) and multiple (recrossing, red dots) TPs, where the TP time τ_{TP} is defined by the turning points of the TPs. It is seen that multiple TPs that consist of recrossing trajectories are significantly faster than single TPs, which reflects that recrossing

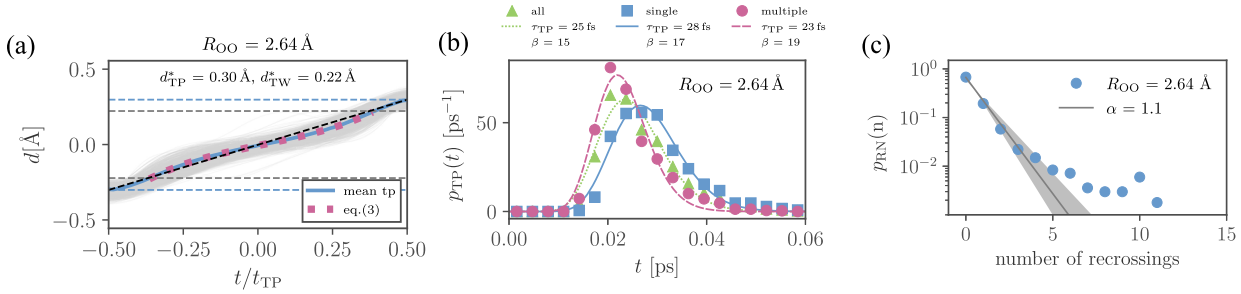

FIG. 3. TP statistics. (a) Ensemble of all 2829 proton TPs for constrained $R_{OO} = 2.64$ Å (gray lines) as a function of the rescaled time t/t_{TP}, where t_{TP} is the individual TP time. The horizontal blue broken lines indicate the mean TP terminal positions $\pm d^*_{TP}/2$, defined by the TP turning points, while horizontal grey dashed lines indicate the free-energy minima $\pm d^*_{TW}/2$. The simulated mean TP (blue line) agrees well with the path-integral prediction Eq. (3) (red dotted line). The straight black broken line also approximates the TP shape quite well. (b) Time distribution p_{TP} of all TPs (green triangles) and a decomposition into single (non-recrossing, blue squares) and multiple (recrossing, red dots) TPs together with fits according to Eq. (4). (c) Recrossing-number probability distribution $p_{RN}(n)$ compared to an exponential fit $p_{RN}(n) = (1 - e^{-\alpha})e^{-\alpha n}$, the confidence interval $\alpha \pm 20\%$ is shown by grey lines.

protons have a higher kinetic energy and, thereby, tend to rebounce back over the barrier. Fits according to the Erlang distribution,[57]

$$p_{TP}(t) = \frac{t^{\beta-1}}{(\beta-1)!}\left(\frac{\beta}{\tau_{TP}}\right)^{\beta} e^{-\beta t/\tau_{TP}}, \tag{4}$$

are shown as lines. In Fig. 3(c) the simulated recrossing-number distribution $p_{RN}(n)$ is compared to an exponential fit with a decay constant $\alpha = 1.1$, 40% of all TPs are single transfer events, $n = 0$, while the remaining 60% TPs are part of multiple events with $n > 0$.

Combining the TP time distribution $p_{TP}(t)$ in the infinitely sharp limit $\beta \to \infty$, the exponential recrossing-number distribution $p_{RN}(n)$ and approximating the TP shape as a straight line, the analytical result for the TP spectral contribution [red broken line in Fig. 2(b3)] is derived in the supplementary material, Sec. XII, and is given as

$$\omega\tilde{\chi}''_{TP}(\omega) = \frac{{d^*_{TP}}^2 q^2}{V\epsilon_0 k_B T \tau_{TW}} \frac{64\omega^2\tau_{TP}^2}{\pi^4(\pi+\omega\tau_{TP})^2} \times \frac{e^{\alpha}\omega^2\tau_{TP}^2}{2\cosh(\alpha) - 2 + (\pi - \omega\tau_{TP})^2}, \tag{5}$$

it matches the simulation data (blue solid line) around the maximum quite well. In the comparison, the mean time of recrossing TPs $\tau_{TP} = 23$ fs from Fig. 3(b) is used, which is shown to be the dominating time scale in the supplementary material, Sec. XII. Interestingly, the TP spectrum Eq. (5) is a product of a Debye and a Lorentzian line shape, both with the same characteristic frequency $f_{TP} = 1/(2\tau_{TP})$, which explains its relative sharpness.

The remaining normal-mode contribution $\tilde{\chi}''_{NM}$ in Fig. 2(b4) is obtained by harmonic analysis of the minimal energy structure, including line broadening from frictional damping (red broken line). The two dominant normal modes around 1416 and 1659 cm^{-1}, which correspond to in-phase and out-of-phase coupled vibrations of the excess protons with the hydrogens of the distant water, are illustrated in Fig. 2(b4) (see Sec. III A and the supplementary material, Sec. III, for details).

In Fig. 2(b1), the simulated excess-proton spectrum (blue solid line) is compared to the sum of the theoretical transfer-waiting, TP, and normal mode predictions (red broken line); the agreement is good (except for very high frequencies), which demonstrates that Eqs. (1) and (5) together with the normal-mode analysis allow us to quantitatively describe excess-proton transfer spectra.

The excess-proton spectra in Fig. 4(a1) vary significantly for different values of R_{OO}. The excess-proton free energies from simulations in Fig. 4(b) demonstrate that the three systems exhibit high, moderate, and low barriers. Very pronounced is the change of the low-frequency shoulder of the transfer-waiting contribution in Fig. 4(a2), which moves to lower frequencies and becomes weaker with growing barrier height and is well captured by the theoretical predictions Eq. (1) (black broken lines), using bi-exponential fits to the transfer-waiting distributions in Fig. 4(c). Equation (2) demonstrates that the spectral differences are due to less frequent transfers as the barrier height increases. The simulated mean transfer-waiting time τ_{TW} in the inset of Fig. 4(c) exponentially increases with the barrier height U_0, as expected for thermally activated barrier crossing.[44,46] On the other hand, the frequency of the TP spectral contribution in Fig. 4(a3) shifts very little for different R_{OO}, which is well-captured by Eq. (5) (black broken lines) and reflects the weak dependence of the TP time τ_{TP} on the barrier height in the inset of Fig. 4(c), in agreement with the predicted logarithmic dependence of τ_{TP} on the barrier height.[49]

Figure 4(d) compares the IR spectrum of the excess proton (blue solid line) in the $H_5O_2^+$ cation to the normal-mode spectrum, including frictional line broadening (grey broken line, see the supplementary material, Sec. III, for details) for fixed $R_{OO} = 2.40$ Å, the barrier-less global minimum of the unconstrained $H_5O_2^+$ cation. The good agreement highlights that the barrier-less Zundel state is well described by a normal-mode analysis. This is in contrast to the results for larger values of R_{OO} in Fig. 4(a), where a finite barrier exists and the transfer-waiting and TP spectral signatures dominate over the normal-mode contribution.

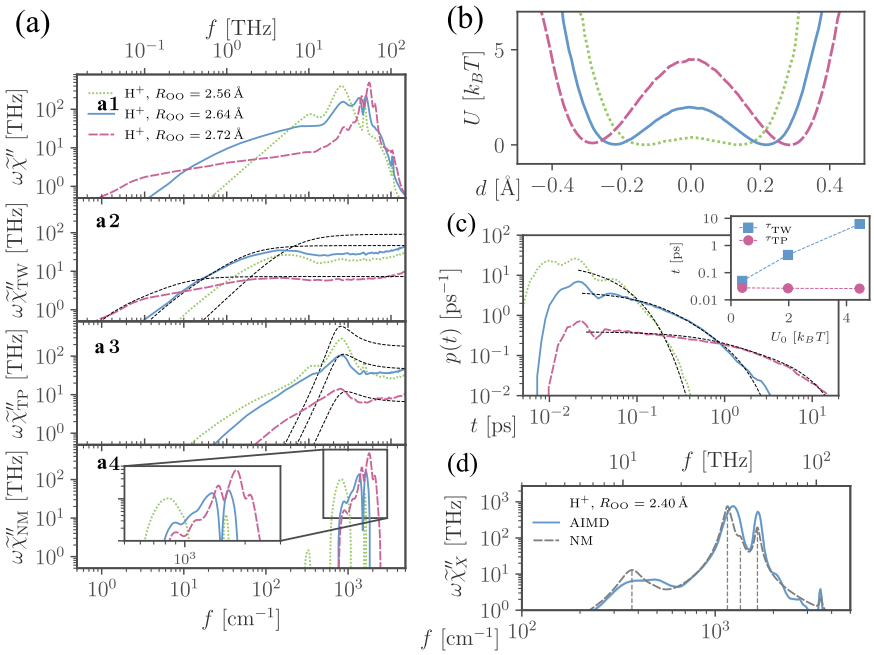

FIG. 4. Decomposition of the excess-proton spectra for various constrained R_{OO}. (a) AIMD spectra are shown as colored lines and theoretical predictions are shown for the transfer-waiting contribution, Eq. (1), in (a2) and for the TP contribution, Eq. (5), in (a3) as thin black broken lines. (a4) shows the normal-mode contributions. See the supplementary material, Sec. XIII, for details. (b) Proton free energies landscapes extracted from simulation trajectories. (c) Transfer-waiting-time distributions together with bi-exponential fits (black broken lines). The inset shows the mean transfer-waiting times τ_{TW} and the mean TP times τ_{TP} as a function of the free-energy barrier height U_0. (d) IR spectrum of the excess proton (blue solid line) in the $H_5O_2^+$ cation with a fixed R_{OO} = 2.40 Å compared to the normal-mode spectrum including frictional line-broadening (grey broken line). Vertical grey broken lines denote the dominant normal modes.

III. CONCLUSIONS AND DISCUSSION

In contrast to traditional normal-mode-based approaches to proton-transfer spectroscopy, which consider proton vibrations around energy minima, we here investigate the spectrum of a proton as it actually makes the move from one energy minimum to another. While the normal-mode frequencies are on the harmonic-approximation level determined by the positive curvature of the energy landscape and by the effective mass, two fundamentally different time scales govern the barrier-crossing absorption spectrum: the mean time the proton waits in a potential minimum before it crosses the barrier, the transfer-waiting time, and the mean time it takes the proton to actually move over the barrier once it has left the potential minimum, the so-called transfer-path (TP) time. While the TP time distribution is rather narrow, which leads to a well-defined TP band, the transfer-waiting times are broadly distributed, which leads to a wide spectral absorption down to low frequencies. Recent experimental studies on hydrochloric acid solutions in the THz regime indeed observed broad absorption that, by comparison with AIMD simulations, could be attributed to proton motion.[52,53]

The AIMD simulations of single $H_5O_2^+$ cations reveal a high similarity between excess-proton-only spectra and spectra from all nuclei and electronic polarizations. This emphasizes the impact of proton-transfer processes on experimentally measured spectra and allows us in turn to develop a stochastic spectral theory based on excess-proton motion only. The excess-proton transfer between two water molecules depends strongly on the separation of the two water oxygens. For oxygen–oxygen separations $R_{OO} \geq 2.5$ Å, a barrier crossing is involved, whereas for closer separations the proton is rather located directly in between the two water molecules. It should be noted, though, that nuclear quantum effects significantly increase the probability to finding the proton in the barrier position, which is typically interpreted as an indication that the effective barrier height is reduced. This means that the effective barrier heights could be smaller in the presence of nuclear quantum effects.

An H/D isotope exchange of the excess proton does not shift the low-frequency transfer-waiting signature, as shown in the supplementary material, Sec. XIV, which is expected since the excess-proton barrier crossing is a friction-dominated process and mass plays only a minor role, as discussed in the supplementary material, Sec. XV. In contrast, TP and normal-mode signatures show isotope effects, which suggests how to experimentally distinguish barrier crossing from the other spectral contributions. For the normal-mode spectral contribution the isotope effect is well known (see Sec. X in the supplementary material), the mass-dependence of the TP spectral contribution is rather subtle and depends on the stochastic mass-friction balance (see Sec. XV in the supplementary material).

The spectroscopic signatures of proton transfer are most pronounced along the transfer direction, as shown in Sec. V in the supplementary material, thus dichroic spectroscopic measurements of oriented samples[33,38] would be most suitable to observe the features discussed in this paper.

A. Methods

The Born–Oppenheimer AIMD simulations of the $H_5O_2^+$ cation were performed with the CP2K 4.1 software package using a doubly polarizable triple-zeta basis set for the valence electrons, dual-space pseudopotentials, the BLYP exchange-correlation functional and D3 dispersion correction.[58–60] The simulation box size was $10 \times 10 \times 10$ Å^3 and the cutoff for the plane-wave representation was 400 Ry. For each constrained system, 20 ps simulations with a time step of 0.5 fs were performed under NVT conditions

at 300 K by coupling all atoms to a CSVR thermostat with a time constant of 100 fs, which has been shown to be exceptionally good for preserving vibrational dynamics.[61] Consequently, a number of independent simulations with a time step of 0.25 fs were performed under NVE conditions starting from different snapshots of the NVT data, 12 × 20 ps for the systems with $R_{OO} \leq 2.5$ Å and ≥20 × 60 ps for the systems with $R_{OO} \geq 2.5$ Å, 20 × 90 ps for $R_{OO} = 2.72$ Å. Even though the time step was chosen to be very small, some systems did not preserve energy during the NVE simulation due to unfavorable starting conditions and the small number of degrees of freedom. These systems were excluded from further analysis. The data for systems with constrained oxygen atoms stem from NVE simulations, totaling in simulation time 240–1800 ps for each system. In the case of the unconstrained system, the oxygen atoms were only constrained in the *yz*-plane. Nevertheless, the NVE simulations were less stable due to large spatial fluctuations along *x*. For this system, NVT simulations with a total simulation time of 20 ps were performed.

Linear response theory relates the dielectric susceptibility $\chi(t)$ to the equilibrium autocorrelation of the dipole moment $C(t) = \langle \boldsymbol{p}(t)\boldsymbol{p}(0)\rangle$, reading in Fourier space

$$\widetilde{\chi}(\omega) = \frac{1}{V\epsilon_0 k_B T}\left(C(0) - i\frac{\omega}{2}\widetilde{C}^{+}(\omega)\right), \tag{6}$$

with system volume V, thermal energy $k_B T$, and vacuum permittivity ϵ_0. IR spectra can therefore be calculated straight-forwardly from sufficiently sampled trajectories of the AIMD simulation data using Eq. (6) and the Wiener-Kintchin relation, derived in the supplementary material, Sec. XVI. Quantum corrections have previously been addressed,[62] but they were not applied here. The dipole moments were obtained after Wannier-center localization of the electron density at a time resolution of 2 fs. The power spectra were smoothed using Gaussian kernels with widths that are logarithmically increasing from 20 cm^{-1} centered at $f = 20$ cm^{-1} to 100 cm^{-1} centered at $f = 5000$ cm^{-1}. All presented spectra were scaled by the volume of two water molecules, $V = 0.060$ nm^3, which follows from the density of water at atmospheric pressure and 300 K, $\rho = 0.99$ g/ml. The normal-mode analysis was performed using the implementation in CP2K 4.1 by diagonalizing the Hessian of energetically optimal structures for the same system parameters as in the AIMD simulations. The normal modes were obtained as the Eigenvectors of the Hessian, the Eigenvalues are the frequencies. A projection of the Eigenvectors onto the excess-proton coordinate gave their spectral contributions. Line broadening resulted from frictional damping with the same fitted friction coefficient $\gamma = 16$ u/ps for all normal modes (see the supplementary material, Sec. X, for details).

SUPPLEMENTARY MATERIAL

See the supplementary material for detailed derivations, analysis procedures, additional data, and discussion.

ACKNOWLEDGMENTS

We gratefully acknowledge support by the DFG (Grant No. SFB 1078), project C1, and computing time on the HPC clusters at the physics department and ZEDAT, FU Berlin. W.K.K. acknowledges the support by a KIAS Individual Grant (No. CG076001) at Korea Institute for Advanced Study.

AUTHOR DECLARATIONS

Conflict of Interest

The authors have no conflicts to disclose.

Author Contributions

F.N.B. and R.R.N. conceived the theory and designed the simulations. F.N.B. performed the AIMD simulations and analyzed the data. P.H. performed the quantummechanical zero-point calculations. W.K.K. contributed to the transfer-path-shape theory. All authors discussed the results, analyses and interpretations. F.N.B. and R.R.N. wrote the paper with input from all authors.

Florian N. Brünig: Conceptualization (equal); Data curation (lead); Formal analysis (equal); Investigation (equal); Methodology (equal); Software (lead); Visualization (lead); Writing – original draft (equal); Writing – review & editing (equal). **Paul Hillmann**: Formal analysis (supporting); Software (supporting); Visualization (supporting); Writing – original draft (supporting). **Won Kyu Kim**: Formal analysis (supporting); Visualization (supporting); Writing – original draft (supporting). **Jan O. Daldrop**: Conceptualization (supporting); Supervision (supporting). **Roland R. Netz**: Conceptualization (equal); Funding acquisition (lead); Project administration (lead); Supervision (lead); Writing – original draft (equal); Writing – review & editing (equal); Formal analysis (equal); Investigation (equal); Methodology (equal).

DATA AVAILABILITY

The data that support the findings of this study are available from the corresponding author upon request.

REFERENCES

[1] D. Marx, "Proton Transfer 200 Years after von Grotthuss: Insights from Ab Initio Simulations," ChemPhysChem **7**, 1848–1870 (2006).
[2] G. Zundel and H. Metzger, Z. Phys. Chem **58**, 225 (1968).
[3] E. Wicke, M. Eigen, and T. Ackermann, Z. Phys. Chem. **1**, 340 (1954).
[4] M. Tuckerman, K. Laasonen, M. Sprik, and M. Parrinello, J. Phys. Chem. **103**, 150 (1995).
[5] T. C. Berkelbach, H.-S. Lee, and M. E. Tuckerman, Phys. Rev. Lett. **103**, 238302 (2009).
[6] D. Asthagiri, L. R. Pratt, and J. D. Kress, Proc. Natl. Acad. Sci. U. S. A. **102**, 6704 (2005).
[7] C. A. Daly, L. M. Streacker, Y. Sun, S. R. Pattenaude, A. A. Hassanali, P. B. Petersen, S. A. Corcelli, and D. Ben-Amotz, J. Phys. Chem. Lett. **8**, 5246 (2017).
[8] F. Dahms, B. P. Fingerhut, E. T. J. Nibbering, E. Pines, and T. Elsaesser, Science **357**, 491 (2017).
[9] W. B. Carpenter, J. A. Fournier, N. H. C. Lewis, and A. Tokmakoff, J. Phys. Chem. B **122**, 2792 (2018).
[10] P. B. Calio, C. Li, and G. A. Voth, J. Am. Chem. Soc. **143**, 18672 (2021).
[11] M. Thämer, L. De Marco, K. Ramasesha, A. Mandal, and A. Tokmakoff, Science **350**, 78 (2015).
[12] J. A. Fournier, W. B. Carpenter, N. H. C. Lewis, and A. Tokmakoff, Nat. Chem. **10**, 932 (2018).

[13]A. Kundu, F. Dahms, B. P. Fingerhut, E. T. J. Nibbering, E. Pines, and T. Elsaesser, J. Phys. Chem. Lett. **10**, 2287 (2019).
[14]W. B. Carpenter, Q. Yu, J. H. Hack, B. Dereka, J. M. Bowman, and A. Tokmakoff, J. Chem. Phys. **153**, 124506 (2020).
[15]D. Marx, M. E. Tuckerman, J. Hutter, and M. Parrinello, Nature **397**, 601 (1999).
[16]J. A. Napoli, O. Marsalek, and T. E. Markland, J. Chem. Phys. **148**, 222833 (2018).
[17]S. Roy, G. K. Schenter, J. A. Napoli, M. D. Baer, T. E. Markland, and C. J. Mundy, J. Phys. Chem. B **124**, 5665 (2020).
[18]T. Komatsuzaki and I. Ohmine, Chem. Phys. **180**, 239 (1994).
[19]W. Kulig and N. Agmon, Nat. Chem. **5**, 29 (2013).
[20]R. Biswas, W. Carpenter, J. A. Fournier, G. A. Voth, and A. Tokmakoff, J. Chem. Phys. **146**, 154507 (2017).
[21]H. Wang and N. Agmon, J. Phys. Chem. A **121**, 3056 (2017).
[22]T. K. Esser, H. Knorke, K. R. Asmis, W. Schöllkopf, Q. Yu, C. Qu, J. M. Bowman, and M. Kaledin, J. Phys. Chem. Lett. **9**, 798 (2018).
[23]S. A. Fischer and D. Gunlycke, J. Phys. Chem. B **123**, 5536 (2019).
[24]K. R. Asmis, N. L. Pivonka, G. Santambrogio, M. Brümmer, C. Kaposta, D. M. Neumark, and L. Wöste, Science **299**, 1375 (2003).
[25]J. M. Headrick, E. G. Diken, R. S. Walters, N. I. Hammer, R. A. Christie, J. Cui, E. M. Myshakin, M. A. Duncan, M. A. Johnson, and K. D. Jordan, Science **308**, 1765 (2005).
[26]T. L. Guasco, M. A. Johnson, and A. B. McCoy, J. Phys. Chem. A **115**, 5847 (2011).
[27]F. Dahms, R. Costard, E. Pines, B. P. Fingerhut, E. T. J. Nibbering, and T. Elsaesser, Angew. Chem., Int. Ed. **55**, 10600 (2016).
[28]M. E. Tuckerman, D. Marx, M. L. Klein, and M. Parrinello, Science **275**, 817 (1997).
[29]J. Sauer and J. Döbler, ChemPhysChem **6**, 1706 (2005).
[30]O. Vendrell, F. Gatti, and H.-D. Meyer, J. Chem. Phys. **127**, 184303 (2007).
[31]F. Agostini, R. Vuilleumier, and G. Ciccotti, J. Chem. Phys. **134**, 084303 (2011).
[32]M. Rossi, M. Ceriotti, and D. E. Manolopoulos, J. Chem. Phys. **140**, 234116 (2014).
[33]J. O. Daldrop, M. Saita, M. Heyden, V. A. Lorenz-Fonfria, J. Heberle, and R. R. Netz, Nat. Commun. **9**, 311 (2018).
[34]C. T. Wolke, J. A. Fournier, L. C. Dzugan, M. R. Fagiani, T. T. Odbadrakh, H. Knorke, K. D. Jordan, A. B. McCoy, K. R. Asmis, and M. A. Johnson, Science **354**, 1131 (2016).
[35]S. Wolf, E. Freier, M. Potschies, E. Hofmann, and K. Gerwert, Angew. Chem., Int. Ed. **49**, 6889 (2010).
[36]R. Tripathi, H. Forbert, and D. Marx, J. Phys. Chem. B **123**, 9598 (2019).
[37]D. Friedrich, F. N. Brünig, A. J. Nieuwkoop, R. R. Netz, P. Hegemann, and H. Oschkinat, Commun. Biol. **3**, 4 (2020).
[38]Y. Yang, T. Stensitzki, L. Sauthof, A. Schmidt, P. Piwowarski, F. Velazquez Escobar, N. Michael, A. D. Nguyen, M. Szczepek, F. N. Brünig, R. R. Netz, M. A. Mroginski, S. Adam, F. Bartl, I. Schapiro, P. Hildebrandt, P. Scheerer, and K. Heyne, Nat. Chem. **14**, 823 (2022).
[39]R. J. Saykally, Science **239**, 157 (1988).
[40]A. Barth, Biochim. Biophys. Acta - Bioenerg. **1767**, 1073 (2007).
[41]M. Park, I. Shin, N. J. Singh, and K. S. Kim, J. Phys. Chem. A **111**, 10692 (2007).
[42]F. Agostini, R. Vuilleumier, and G. Ciccotti, J. Chem. Phys. **134**, 084302 (2011).
[43]F. N. Brünig, O. Geburtig, A. von Canal, J. Kappler, and R. R. Netz, J. Phys. Chem. B **126**, 1579 (2022).
[44]H. A. Kramers, Physica **7**, 284 (1940).
[45]G. Williams, Chem. Rev. **72**, 55 (1972).
[46]J. Kappler, J. O. Daldrop, F. N. Brünig, M. D. Boehle, and R. R. Netz, J. Chem. Phys. **148**, 014903 (2018).
[47]G. Hummer, J. Chem. Phys. **120**, 516 (2004).
[48]P. Faccioli, M. Sega, F. Pederiva, and H. Orland, Phys. Rev. Lett. **97**, 108101 (2006).
[49]H. S. Chung, J. M. Louis, and W. A. Eaton, Proc. Natl. Acad. Sci. U. S. A. **106**, 11837 (2009).
[50]W. K. Kim and R. R. Netz, J. Chem. Phys. **143**, 224108 (2015).
[51]P. Cossio, G. Hummer, and A. Szabo, J. Chem. Phys. **148**, 123309 (2018).
[52]D. Decka, G. Schwaab, and M. Havenith, Phys. Chem. Chem. Phys. **17**, 11898 (2015).
[53]F. N. Brünig, M. Rammler, E. M. Adams, M. Havenith, and R. R. Netz, Nat. Commun. **13**, 4210 (2022).
[54]C. Schran and D. Marx, Phys. Chem. Chem. Phys. **21**, 24967 (2019).
[55]M. Sprik and G. Ciccotti, J. Chem. Phys. **109**, 7737 (1998).
[56]J. O. Daldrop, W. K. Kim, and R. R. Netz, Europhys. Lett. **113**, 18004 (2016).
[57]D. R. Cox and H. D. Miller, *The Theory of Stochastic Processes* (CRC Press, 1977).
[58]J. Hutter, M. Iannuzzi, F. Schiffmann, and J. Vandevondele, Wiley Interdiscip. Rev.: Comput. Mol. Sci. **4**, 15 (2014).
[59]R. A. Kendall, T. H. Dunning, and R. J. Harrison, J. Chem. Phys. **96**, 6796 (1992).
[60]S. Grimme, J. Antony, S. Ehrlich, and H. Krieg, J. Chem. Phys. **132**, 154104 (2010).
[61]G. Bussi, D. Donadio, and M. Parrinello, J. Chem. Phys. **126**, 014101 (2007).
[62]R. Ramírez, T. López-Ciudad, P. Kumar P, and D. Marx, J. Chem. Phys. **121**, 3973 (2004).